Title:

A general model of locomotion of brittle stars with a variable number of arms

Running head:

General model of locomotion of brittle stars

Author names and institutional addresses:

Daiki WAKITA[1], Katsushi KAGAYA[2,3], Hitoshi AONUMA[1,4*]

[1]Graduate School of Life Science; Hokkaido University; Sapporo, Hokkaido, 060-0810; Japan; dwntzrd@gmail.com

[2]The Hakubi Center for Advanced Research; Kyoto University; Yoshida-Konoe, Kyoto, 606-8501; Japan; kagaya.katsushi.8e@kyoto-u.ac.jp

[3]Seto Marine Biological Laboratory, Field Science, Education and Research Center; Kyoto University; Shirahama, Wakayama, 649-2211; Japan

[4]Research Institute for Electronic Science; Hokkaido University; Sapporo, Hokkaido, 060-0812; Japan; aon@es.hokudai.ac.jp

[*]**Corresponding author:**

Hitoshi Aonuma

Research Center of Mathematics for Social Creativity, Research Institute for Electronic Science, Hokkaido University, Sapporo 060-0812, Japan.

Tel/Fax: +81-11-706-3832

Email: aon@es.hokudai.ac.jp

Abstract

Typical brittle stars have five radially symmetrical arms that coordinate to move the body in a certain direction. However, some species have a variable number of arms, which is a unique trait since intact animals normally have a fixed number of limbs. How does a single species manage different numbers of appendages for adaptive locomotion? We herein describe locomotion in *Ophiactis brachyaspis* with four, five, six, and seven arms to propose a common rule for the movement of brittle stars with different numbers of arms. For this, we mechanically stimulated one arm of individuals to analyse escape direction and arm movement. By gathering quantitative indices and employing Bayesian statistical modelling, we noted a pattern: regardless of the total number of arms, an anterior position emerges at one of the second neighbouring arms to a mechanically stimulated arm, while arms adjacent to the anterior one synchronously work as left and right rowers. We propose a model in which an afferent signal runs clockwise or anticlockwise along the nerve ring while linearly counting how many arms it passes through. With this model, the question on how ‘left and right’ emerges in a radially symmetrical body via a decentralized system is answered.

Keywords

echinoderm, radial symmetry, movement coordination, escape direction, Bayesian statistical modelling, WAIC

Introduction

Legged animals use appendages to move around on the ground. In most cases, intact adults of a species have a constant number of limbs; most mammals, for instance, have four limbs, whereas most insects have six. These species supposedly use a number-specific mechanism of locomotion. In contrast, in some species of brittle stars (Echinodermata: Ophiuroidea), some intact individuals have five appendages or less, whereas others have six or more (Fig. 1). This variability usually occurs in fissiparous species, which undergo asexual reproduction by fission and regeneration (Boffi, 1972; Mladenov et al., 1983; Mladenov and Emson, 1984).

Similar to typical echinoderms that show pentaradial symmetry, most ophiuroid species have five multi-jointed appendages called ‘arms’, which extend from the ‘disk’ at the centre of the animal. Previous studies have described arm movements in the locomotion of five-armed species in qualitative terms (Romanes and Ewart, 1881; Preyer, 1887; Uexküll, 1905; Glaser, 1907; Arshavskii et al., 1976a,b; Clark et al., 2019; Kano et al., 2019) as well as in quantitative terms (Astley, 2012; Kano et al., 2017). Several locomotion modes have been known to occur even in a single species. An often reported mode, referred to as “breast stroke” (Arshavskii et al., 1976a,b) or “rowing” (Astley, 2012), is characterized by a leading arm facing forward, two side arms working as left and right rowers, and two back arms being dragged passively (Romanes and Ewart, 1881; Preyer, 1887; Glaser, 1907; Arshavskii et al., 1976a,b; Astley, 2012; Kano et al., 2017). Some studies have reported another locomotion mode, called “paddling” (Arshavskii et al., 1976a) or “reverse rowing” (Astley, 2012), in which a backmost arm is dragged while the other four actively row (Preyer, 1887; Uexküll, 1905; Glaser, 1907; Arshavskii et al., 1976a; Astley, 2012). These bilaterally coordinated movements enable the ophiuroid body to creep in a certain direction (Astley, 2012). Nevertheless, since the role of each arm switches as the body changes moving direction (Arshavskii et al., 1976a; Astley, 2012), brittle stars do not have consistent antero-posterior and left-right axes.

The ophiuroid nervous system mainly comprises a circumoral nerve ring in the disk and radial nerve cords running into each arm (Cobb and Stubbs, 1981, 1982; Ghyoot et al., 1994; Bremaeker et al., 1997; Zueva et al., 2018). At each branch point to

the radial nerve, the nerve ring has regional concentrations of neural cell bodies (i.e., ganglia) that control some organs (Ghyoot et al., 1994). Some behavioural studies have supported the essential role of the nerve ring in locomotion. For instance, menthol-anaesthetic experiments described the nerve ring's function in initiating locomotion (Matsuzaka et al., 2017), whereas nerve cut experiments demonstrated its role in arm coordination (Mangold, 1909; Diebschlag, 1938; Arshavskii et al., 1976a,b; Clark et al., 2019; Kano et al., 2019).

Although locomotion in common five-armed brittle stars and the morphological variability in some species have been studied in different contexts, no study has focused locomotion of ophiuroids with different numbers of arms. Some studies have described locomotion with several severed arms (Arshavskii et al., 1976b; Kano et al., 2017; Matsuzaka et al., 2017; Clark et al., 2019); however, in these cases, the pentaradial architecture remained at the disk, including the nerve ring. When the structural division differs at the centre of the animal, the nerve ring must have a different number of branches connecting it to the radial nerves, i.e., a different number of ganglia. Given the reported importance of the nerve ring in locomotion, this difference must result in a huge issue regarding the integration of the individual.

Therefore, the aim of our study was to understand how a species adapts its locomotion to a changeable number of limbs and network branches, and to propose a model for ophiuroid locomotion considering the varying number of radially symmetrical arms. For this, we targeted four-, five-, six-, and seven-armed intact individuals of the fissiparous species *Ophiactis brachyaspis* Clark, 1911 (Fig. 1). For probing into inter-arm communication, an aversive tactile stimulus was applied on one arm and the reactions of the other arms were observed. Although electrophysiological approaches are difficult in the small body of fissiparous ophiuroids, we expected each arm's movement to be a simple reflection of neural activity; therefore, external behavioural modelling will infer internal neural networks. Our primary hypothesis was that brittle stars would have a decentralized nervous system, as suggested by previous studies. Matsuzaka et al. (2017), for instance, observed that unanaesthetized arms carried food to the mouth in the wholly anaesthetized disk; Kano et al. (2019) cut the nerve ring at two points and observed that two- and three-armed portions within the five-armed body often crept oppositely to each other. To allow the variability of the

total number of arms, each functional unit would neurally affect only the nearest-neighbour units while ignoring distant ones. In a decentralized model, we would expect a threat to an arm to make its both neighbours push toward the stimulus so that the disk can escape in the direction opposite to the stimulus, as shown in Kano et al.'s (2019) model.

We herein quantitatively described post-stimulus locomotion based on arm movements and escape direction, employing Bayesian estimation and model evaluation to understand their potential structures as reasonable distributions. Our results indeed reinforced the support of a decentralized strategy in the ophiuroid body; however, contrary to our initial expectation, escape direction was not always the opposite of the stimulation direction. We thus suggest the following model: a threat to an arm makes an afferent signal that asymmetrically dominates (in clockwise or anticlockwise direction) the nerve ring; in the same direction, the stimulated arm's *second* neighbouring arm is highly probable to be the leading arm, with the leader's side arms working as left and right synchronous rowers. Thus, regardless of the total number of arms, ophiuroid locomotion shows a common anterior pattern, which could be positioned by linearly counting how many arms some signal passes in one direction along a circular pathway. We provide a unique idea of how a multi-directional body determines a movement direction.

Materials and methods

Animals

The fissiparous brittle star *Ophiactis brachyaspis* (Fig. 1) was used. In nature, this species densely inhabits upper and lateral surfaces of rough rocks or adherent organisms such as sponges. Some of its arms lie in interstices while some rise from the substrate; suspension-feeding ophiuroids show this posture to capture particles (Warner, 1971). Animals collected from Shirahama Aquarium, Kyoto University, were reared in a laboratory aquarium (450 × 450 × 450 mm) filled with artificial seawater at 25–28°C and salinity of 32–35‰ (TetraMarin Salt Pro, Tetra Japan Co, Tokyo, Japan). The body size was 1.5–3.0 mm in disk diameter and 5–15 mm in arm length. Most specimens

(~70%) had six arms and others had five arms. One individual with four arms and another with seven arms, both quite rare, were obtained in this study.

Behavioural experiments

To investigate locomotion, 10 five-armed and 10 six-armed individuals were used. No arm was more than twice the length of the shortest arm in a specimen (c.f. Fig. 1). The four- and seven-armed individuals were also targeted. Each specimen was placed in a horizontal flat acrylic case (105 × 75 × 22 mm) filled with 100 mL of artificial seawater from the laboratory aquarium, with no strong light gradient and no strong current. Locomotion was recorded in aboral view using a digital camera (EOS8000D, Canon, Tokyo, Japan) with videos saved in MP4 format. Aversive tactile stimuli were applied to arms to trigger escape. In each trial, the very tip of an arm was manually tapped on both its lateral faces about four times with the sharp end of a toothpick. The next stimulus was applied at the anticlockwise neighbouring arm after more than two minutes. This rotation order was repeated until all arms of each individual had been stimulated at least three times.

The locomotion for one minute after the disk began to move in response to each stimulus (c.f. Videos S1, S2) was extracted from long-term videos; the disk's movement generally started within ten seconds after stimulation. Per five- or six-armed individual, three trials that showed the longest moving distances of the disk were analysed. For the four- and seven-armed individuals, the 15 trials with the longest moving distances were analysed.

Measurements

To quantify temporal changes in body posture during locomotion, simple feature points that effectively outlined the ophiuroid movements were used. The stimulated arm in each trial was numbered 1, which was followed anticlockwise by the other arms; α is the index of arms (α = 1, 2, 3, 4, 5 in the five-armed instance). Using a semiautomatic tracking software Kinovea ver. 0.8.27 (http://www.kinovea.org/, accessed 4 December 2018), two coordinate points in each arm were traced at 10 f.p.s.: $P_\alpha(t) = (x_\alpha(t), y_\alpha(t))$—which indicates the attachment point of the α-th arm to the disk viewed aborally—and $P'_\alpha(t) = (x'_\alpha(t), y'_\alpha(t))$—which indicates the point at half the length of the α-th arm

considering the range from the disk's centre to the arm tip—at the t-th frame (Fig. 2; t = 1, 2, ..., 600). $P_\alpha(t)$ defined a basal point for each arm. For $P'_\alpha(t)$, i.e., the midpoint of each arm, we did not use the tip of the arm because it may rise or make casual movements irrelevant for locomotion, as indicated by Matsuzaka et al. (2017). $P_{\mathrm{cent}}(t)$ was defined as the centre of gravity of all arm bases (i.e., $P_\alpha(t)$), which is similar to the centre of the disk (Fig. 2).

Based on the abovementioned points (two types of tracked points and one derivative point), we calculated several measurements that provided practical information. The α-th arm's length (L_α) was defined as the maximum length of the segment $P_\alpha(t)P'_\alpha(t)$ in the analysed period; note that L_α was sampled in each trial, thus not accounting for the constant length of each arm. Moving distance (S) was measured as the length of $P_{\mathrm{cent}}(1)P_{\mathrm{cent}}(T)$, where T is the total number of frames, i.e., 600 (Fig. 2).

To understand in what direction the brittle stars escape after aversive stimulation, moving direction (Θ) was assessed as follows:

$$\Theta = \frac{1}{T}\sum_{t=1}^{T}\big(\theta(t)\big) \qquad (1),$$

where $\theta(t)$ is the angle of the two segments $P_{\mathrm{c}}(1)P_{\mathrm{c}}(T)$ and $P_1(t)P_{\mathrm{cent}}(t)$ (Figs 2, 3). Θ, which may be from −180 to 180 deg, is 0 deg when the disk moves in the direction opposite to the stimulated arm. A negative or positive value of Θ indicated that the track of the disk was inclined clockwise or anticlockwise, respectively, from the direction opposite to the stimulated arm. For statistics, the dummy variable Θ_{sign} was defined as:

$$\Theta_{\mathrm{sign}} = \begin{cases} 0 & (-180 \le \Theta < 0) \\ 1 & (0 \le \Theta < 180) \end{cases} \qquad (2).$$

Meanwhile, the movement of each arm during locomotion was calculated. In actively rowing arms, pushing backward was slower on the ground, while returning toward was faster off the ground (c.f. Videos S1, S2). This directionality in arm angular velocity was used to quantify the degree to which each arm functions as a left or right rower. The angular velocity was obtained from arm angle in horizontal terms, informed by the defined points. The long segment $P_{\mathrm{cent}}(t)P'_\alpha(t)$ during locomotion swung around the short one $P_{\mathrm{cent}}(t)P_\alpha(t)$, so each arm's angle at the t-th frame ($\varphi_\alpha(t)$) was defined as the angle formed by these two segments (Fig. 2). The arm angle $\varphi_\alpha(t)$ was negative or positive when $P_{\mathrm{cent}}(t)P'_\alpha(t)$ was angled clockwise or anticlockwise, respectively, from $P_{\mathrm{cent}}(t)P_\alpha(t)$. The arm angular velocity ($\omega_\alpha(t)$) was calculated from $\varphi_\alpha(t)$ with a five-

point moving average method (window size 0.5 s), and then smoothened with a low-pass filter with the cut-off frequency of 1.0 Hz (Fig. 3). The filtered velocity $\omega_\alpha(t)$ was used to evaluate the degree of a leftward or rightward bias in arm movement, which is represented by B_α (named after "bias"; Fig. 3):

$$B_\alpha = \frac{1}{T}\sum_{t=1}^{T}\left(\omega_\alpha(t)^2 \mathrm{sign}\left(\omega_\alpha(t)\right)\right) \quad (3).$$

Assuming that a directional bias results from a speed difference between pushing and returning in each arm, we can rephrase B_α as each arm's tendency of being a left or right rower. A largely negative value of B_α represented that the α-th arm moved clockwise faster than anticlockwise, indicating that it slowly pushed leftward and returned fast rightward viewed proximally from the disk. In contrast, B_α was largely positive when the arm pushed rightward (clockwise). Its value was close to zero when the arm pushed leftward and rightward equally or was dragged without actively returning. Moreover, frequency components in the non-filtered $\omega_\alpha(t)$ of each arm were extracted using Fourier transforms. F_α was defined as the frequency at the peak amplitude in the α-th arm.

To understand how the arms synchronize with each other (i.e., synphase, no synchrony, or antiphase), the filtered velocity $\omega_\alpha(t)$ was used to calculate Kano et al.'s (2017) E_{ij}, namely, the degree of synchronization between two arms:

$$E_{\alpha\beta} = \frac{1}{T}\sum_{t=1}^{T}\omega_\alpha(t)\omega_\beta(t) \quad (4).$$

A negative or positive value of $E_{\alpha\beta}$ indicated that the movements of the α- and β-th arms synchronized in the opposite (antiphase) or same direction (synphase), respectively. A value around zero represented that the two arms move without synchrony or were static.

Statistical modelling

To capture a structure and correlation of measurements, we built multiple hypotheses in the form of probability distribution models regarding Θ, B_α, and $E_{\alpha\beta}$ (explained in this section), and later quantitatively compared how appropriate each hypothesis was using an information criterion (explained in the section "Bayesian inference and model evaluation").

Firstly, we hypothesized that brittle stars were likely to escape in one frequent direction (e.g., the direct opposite of the stimulus) or in two frequent directions. To

examine a possible bimodality in moving direction, we assumed that Θ was subjected to a single von Mises distribution (f_{vM}, 'circular normal distribution'),

$$\Theta[n] \sim f_{\mathrm{vM}}(\mu_\Theta, \kappa_\Theta),\ -\pi \le \mu_\Theta \le \pi,\ \kappa_\Theta \ge 0 \quad (5),$$

or a mixture of two von Mises distributions,

$$\Theta[n] \sim \frac{1}{2} f_{\mathrm{vM}}(-\mu_\Theta, \kappa_\Theta) + \frac{1}{2} f_{\mathrm{vM}}(\mu_\Theta, \kappa_\Theta),\ -\pi \le \mu_\Theta \le \pi,\ \kappa_\Theta \ge 0 \quad (6).$$

Hereafter, n takes one to the total number of trials, so that $\Theta[n]$ denotes the n-th element of Θ. The parameters as random variables μ_Θ—converted to radians for modelling—and κ_Θ were analogous to the mean and the reciprocal of variance, respectively, in a normal distribution. For the mixed case, we assumed that the two distributions were symmetrical to each other with respect to the position of 0 deg.

Secondly, we supposed that the leftward/rightward bias of each arm was associated with another factor such as arm length, moving direction, or some sort of individual difference. To understand what is largely related to a trial-by-trial variability of B_α, we parametrized L_α, S, Θ, Θ_{sign}, and F_α each as an explanatory variable for B_α. We assumed a normal distribution $f_{\mathrm{norm}}(\mu, \sigma)$, where μ and σ respectively represent the mean and standard deviation (s.d.), as follows:

$$B_\alpha[n, \alpha] \sim f_{\mathrm{norm}}(\mu_{\mathrm{Bi}}[\alpha] + \mu_{\mathrm{Bs}}[\alpha]X, \sigma_{\mathrm{Bi}}[\alpha]),\ \sigma_{\mathrm{Bi}} \ge 0 \quad (7).$$

Here, μ_{Bi}, μ_{Bs}, and σ_{Bi} are arm-by-arm parameters and X is an explanatory variable to which $L_\alpha[n, \alpha]$, $S[n]$, $\Theta[n]$, $\Theta_{\mathrm{sign}}[n]$, or $F_\alpha[n, \alpha]$ is assigned. S, Θ, and Θ_{sign} were common values for all the arms in the same trial. The categorical index Θ_{sign} indicates whether B_α varies continuously by Θ or switches discretely by the sign of Θ. When Θ_{sign} stands for X, μ_{Bs} represents the means' difference between the negative and positive cases since this variable disappears if Θ_{sign} is zero ($-180 \le \Theta < 0$) and appears if Θ_{sign} is one ($0 \le \Theta < 180$). The model without the member $\mu_{\mathrm{Bs}}[\alpha]X$, i.e., without explanatory variables, is for comparison. In parallel, as for five- and six-armed animals, it was tested if B_α was well explained by individuality, namely, a quality made by some individual difference other than arm number. Consideration of individuality was given by the mean's intercept μ_{Bi}:

$$\mu_{\mathrm{Bi}}[i, \alpha] \sim f_{\mathrm{norm}}(\mu_{\mathrm{B0}}[\alpha], \sigma_{\mathrm{B0}}),\ \sigma_{\mathrm{B0}} \ge 0 \quad (8),$$

$$B_\alpha[n, \alpha] \sim f_{\mathrm{norm}}(\mu_{\mathrm{Bi}}[i, \alpha] + \mu_{\mathrm{Bs}}[\alpha]X, \sigma_{\mathrm{Bi}}[\alpha]),\ \sigma_{\mathrm{Bi}} \ge 0 \quad (9),$$

where i takes one to the total number of individuals (i.e., 10) and the hyperparameters

μ_{B0} and σ_{B0} are random variables. The parameter σ_{B0}, which is common in all arms, has a weakly informative prior as:

$$\sigma_{B0} \sim f_t^+(3, 0, 20) \quad (10),$$

where f_t^+ denotes the half t distribution and the parenthetical parameters represent the degree of freedom (ν), location (mean when $\nu > 1$), and scale (s.d. divided by $\sqrt{3}$ when $\nu = 3$), respectively.

Thirdly, the degree of synchronization between two arms was expected to be linked with moving distance or direction. Similarly to the models for B_α, a best explanatory variable for $E_{\alpha\beta}$ was explored in four- to seven-armed animals:

$$E_{\alpha\beta}[n,p] \sim f_{\mathrm{norm}}(\mu_{Ei}[p] + \mu_{Es}[p]X, \sigma_{Ei}[p]),\ \sigma_{Ei} \geq 0 \quad (11),$$

where μ_{Ei}, μ_{Es}, and σ_{Ei} are pair-by-pair parameters and the explanatory variable X takes $S[n]$, $\Theta[n]$, or $\Theta_{\mathrm{sign}}[n]$. A model without the explanatory member $\mu_{Es}[p]X$ was also considered. No informative prior was set in all the parameters other than σ_{B0} (Equation 10).

Bayesian inference and model evaluation

The parameters (i.e., lowercase symbols in the models presented above) were estimated by employing the Bayesian approach because most parameters in our model had posterior distributions that could not be approximated using any normal distribution; the maximum likelihood method gives less accurate inference than the Bayesian one in this case (Watanabe, 2018). Especially, in singular models, which contain mixed distribution (c.f. Equation 6) or hierarchical parameters (c.f. Equations 8, 9) for instance, the maximum likelihood estimator often diverges or makes the generalization error very large (Watanabe, 2009, 2010). The Bayesian inference is, however, sensitive to priors and statistical models made by scientists. To evaluate arbitrary pairs of priors and models, we used the Widely Applicable Information Criterion (WAIC), which is appropriate even for singular models (Watanabe, 2009, 2010). Information presented in the Results and Discussion sections is based on the models selected using WAIC.

Bayesian estimation was performed using the no-U-turn sampler (NUTS) (Hoffman and Gelman, 2014)—a variant of the Hamiltonian Monte Carlo (HMC) algorithm. In each sampling, 10,000 NUTS samples were obtained from four Markov

chains, in each of which every 40th generation was sampled in 100,000 iterations after a warmup of 5,000, with the target acceptance rate of 0.8. Convergence of each parameter was checked by trace plots, the potential scale reduction factor $\hat{R} \leq 1.1$, and the effective sample size $\hat{n}_{eff} \geq 40$, i.e., at least 10 per chain (Gelman et al., 2013).

The resultant statements were developed according to better prediction models, which yielded smaller WAICs than the others considered. For comparison between models, we referred to the difference as:

$$\Delta = 2N(W - W_{\min}) \qquad (12),$$

where N is the total number of measured samples; multiplication by $2N$ is for the AIC scaling (Gelman et al., 2013). W is the WAIC of a given model while $W_{\min}$ is the smallest WAIC among those of the proposed models; Δ is zero in a best performed models. For presenting figures, the posterior predictive distributions of Θ are shown based on the parameters' posterior distributions in a best model, each indicating a probability distribution which is expected to generate a random variable in a new trial. To visualize B_α and $E_{\alpha\beta}$ dependent on a best explanatory variable, the median of each posterior distribution was obtained under a model including the explanatory variable not only in the mean but also in the s.d.; Equation 7 or 9 was modified to:

$$B_\alpha[n,\alpha] \sim f_{\mathrm{norm}}(\mu_{\mathrm{Bi}}[\alpha] + \mu_{\mathrm{Bs}}[\alpha]X, \exp(\sigma'_{\mathrm{Bi}}[\alpha] + \sigma'_{\mathrm{Bs}}[\alpha]X)) \qquad (13),$$

while Equation 11 was replaced by:

$$E_{\alpha\beta}[n,p] \sim f_{\mathrm{norm}}(\mu_{\mathrm{Ei}}[p] + \mu_{\mathrm{Es}}[p]X, \exp(\sigma'_{\mathrm{Ei}}[p] + \sigma'_{\mathrm{Es}}[p]X)) \qquad (14).$$

Exponentiation in scale makes the s.d. positive while σ'_{Bi}, σ'_{Bs}, σ'_{Ei}, and σ'_{Es} are random variables without constraints. We did not consider scale's explanatory variables when comparing WAICs because the Markov chain simulation failed to converge in many cases. Statistical computation was performed in the software environment R ver. 3.5.1 (R Core Team, 2018), in which Stan codes were compiled and executed using the R package "rstan" (Stan Development Team, 2018). All source codes and data are available from the Figshare repository (Wakita et al., 2019b).

Results

Moving direction (Θ)

The post-stimulus moving direction Θ (Figs 2, 3; Equation 1 in "Materials and methods") are shown in Fig. 4 by dot plots. For all the four-, five-, six-, and seven-armed cases, based on the evaluation using WAIC, the results of Θ were better explained by the model assuming a mixture of two distributions than that assuming a single distribution (Table 1; note that a model with a smaller WAIC better predicts data than a model with a higher WAIC). In other words, it is likely that brittle stars showed two frequent escape directions rather than one. Compared to the four- and five-armed animals, the six- and seven-armed ones had larger differences of WAIC between one- and two-distribution models—represented by Δ in Table 1 (Equation 12). This indicates that the tendency for bimodality increased with number of arms. Following the better model in terms of WAIC, we hereafter show the results on the assumption of two frequent moving directions for all the cases.

The two peak locations were ±17, ±29, ±46, and ±70 deg in four-, five-, six, and seven-armed animals, respectively, informed by the posterior medians of means (μ_Θ) calculated separately for the negative and positive ranges. These estimated values indicate that the more arms a brittle star had, the further the two distributions of Θ were apart from each other (Fig. 4). In other words, the average moving direction of individuals with more arms was more inclined from the direction opposite to the stimulated arm. The predictive distribution of Θ indeed depicted this trend (Fig. 4).

Left or right rower (B_α)

B_α—each arm's tendency of being a left or right rower (Figs 2, 3; Equation 3)—are schematized trial-by-trial in Figs S1–S4. As for the five- and six-armed populations, no-individuality models were consistently better evaluated than their counterparts in which individuality was assigned to the mean of B_α (Table 1). We thus avoid mentioning individual difference within the same arm number.

Scatter diagrams between the principal components of B_α and other measurements are summarized in Fig. S5. Among L_α, S, Θ, Θ_{sign}, F_α, and no explanatory variable, the arm bias B_α in five-armed animals was best explained by the continuous moving direction Θ (Table 1). This means that the side in which each arm rowed was strongly associated with the direction to which the five-armed brittle stars

escaped. As a similar result, the six- and seven-armed cases emphasized the importance of Θ_{sign} (Equation 2), the sign of moving direction in discrete terms. This indicates that the leftward/rightward bias of each arm could be categorized into two groups according to the range in which a six- or seven-armed brittle star escaped to the midline of the stimulated arm. In the four-armed specimen, the arm length L_α was chosen as a best explanatory variable although Θ showed a close performance, implying that each arm's movement bias changed with arm length and/or escape direction. Given the dominance of moving direction as a correlate of B_α, and also given Θ's bimodality (Fig. 4), we present the data of B_α separately by Θ_{sign}—in which side moving direction inclined from the midline of the stimulated arm. Two groups were herein defined based on whether the direction angled clockwise ($\Theta_{\mathrm{sign}} = 0$) or anticlockwise ($\Theta_{\mathrm{sign}} = 1$).

The Θ_{sign}-based grouping exhibited a common locomotion mode among four-, five-, six-, and seven-armed animals in regards to B_α's posterior means. The directional property of each arm could be explained by the number of arms counted from the stimulated arm. Primarily, one of the *first* neighbouring arms to the stimulated arm consistently took the largest or second largest $|B_\alpha|$—absolute values of posterior means (Figs 5–8A,C). This *first* arm corresponded to the anticlockwise neighbour of arm 1 when $\Theta_{\mathrm{sign}} = 0$ (Figs 5–8A) and to the clockwise one when $\Theta_{\mathrm{sign}} = 1$ (Figs 5–8C). The *second* neighbour from the stimulus—next to the *first* in the same direction—took the smallest or second smallest $|B_\alpha|$. Then, the *third* neighbour of the stimulus—next to the *second*—took the largest or second largest $|B_\alpha|$, which was opposite in sign to that of the *first*. One exception was the seven-armed specimen when $\Theta_{\mathrm{sign}} = 0$ (Fig. 8A); the *second* (arm 3) and the *third* (arm 4) neighbours had the fourth smallest and the third largest $|B_\alpha|$, respectively, probably due to the outlying trial shown in row 1 of column 4 (left triangle symbol) in Fig. S4. Replacing the ordinary cases' values with actual movements, the *first* actively pushed in the direction of the stimulated arm, while the *third* actively pushed oppositely to the *first*. These movements could make the *second* face forward, which indeed corresponded to the ranges of Θ in all the cases (Figs 5–8A,C; see also Videos S1, S2).

Synchronization between two arms ($E_{\alpha\beta}$)

The higher explanatory power of Θ_{sign} could also be applied to the instance of the

393 degree of synchronization between the α- and β-th arms, $E_{\alpha\beta}$ (Equation 4), because the
394 five-, six-, and seven-armed cases were each better explained by the model assuming
395 Θ_{sign}'s effect than the others considered (Table 1). Thus, the synchronous movement of
396 each arm with each other could be discretely grouped by in which side a brittle star
397 escaped to the midline of the stimulated arm. In the four-armed animal, the model
398 without an explanatory variable best performed while the presence of Θ or Θ_{sign} resulted
399 in similar performance, implying that arms synchronization was not strongly related to
400 the measurements considered or was altered by the body's moving direction. Accenting
401 the significance of Θ_{sign} as with B_α's situation, we here show the resultant values of the
402 synchronization degree $E_{\alpha\beta}$ discretely by the sign of moving direction Θ.
403 A side-by-side comparison with the Θ_{sign}-based results of B_α showed us that the
404 pair of the *first* and *third* rowers counting from the stimulus had the largest negative
405 medians of $E_{\alpha\beta}$'s posterior means in most cases (Figs 5–8B,D). Although one exception
406 was found in the seven-armed individual with $\Theta_{\mathrm{sign}} = 0$, the pair's value E_{24} leaned
407 negatively as well (Fig. 8B). These values gave a quantitative indication that these two
408 arms tended to simultaneously push in opposite directions, regardless of the number of
409 arms.
410
411
412 **Discussion**
413
414 In the present study, we newly described the post-stimulus locomotion of brittle stars
415 based on the behaviours of four-, five-, six-, and seven-armed intact individuals of a
416 single species. For this purpose, by not stereotyping a discrete role of each arm, we
417 introduced a quantitative index that represents each arm's tendency of being a left or
418 right rower, namely B_α. Coupled with other supportive values, we propose the following
419 common rule for specimens with different numbers of arms: brittle stars frequently
420 travel in the direction of one of the second neighbouring arms to the stimulated arm (Fig.
421 9). Our behavioural model thus presents a general scheme of how radially symmetrical
422 animals map 'left and right'—or 'front and back'—on its behaviour via a decentralized
423 control.
424

Locomotion modes

Previous quantitative studies using five-armed brittle stars have supported antiphase synchronization of two distant arms by assessing the stop and start timing of arm movements (Astley, 2012) and by evaluating $E_{\alpha\beta}$ (Kano et al., 2017) as in the present study. This locomotion mode, which is referred to as “breast stroke” or “rowing”, is characterized by a leading arm and its side rowing arms (Romanes and Ewart, 1881; Preyer, 1887; Glaser, 1907; Arshavskii et al., 1976a,b; Astley, 2012; Kano et al., 2017; Clark et al., 2019). Our results regarding the five-armed specimens of *Ophiactis brachyaspis*, in which the rowing pair showed a high degree of antiphase synchronization (Fig. 5), agree with Kano et al.’s (2017) results for *Ophiarachna incrassata* based on the commonly used index $E_{\alpha\beta}$. An important outcome of our study is that even four-, six-, and seven-armed brittle stars have the triplet of left-front-right (Figs 6–8A,C), in which the left and right rowers tend to simultaneously push the ground backward (Figs 6–8B,D). This extension suggests that this locomotion mode is determined anteriorly, not laterally or posteriorly. However, the mechanism of synchronization of the left and right arms is still unknown, although we assume that it involves neural circuits that coordinate the anterior union.

The two back arms in the five-armed leading locomotion mode have been often interpreted as passively dragged ones (Romanes and Ewart, 1881; Preyer, 1887; Arshavskii et al., 1976a,b; Watanabe et al., 2011). However, our study showed that these arms rather work as weaker rowers since their B_α values ranged either negatively or positively (Fig. 5A,C). In six- and seven-armed ophiuroids, the back arms following the two strong rowers similarly exhibited a rowing trend, whereas the backmost ones were usually neutral as to the leftward or rightward bias just like the leading arm (Figs 6A,C, 8A,C). Thus, more arms may become ‘rowers’, especially in brittle stars with more arms.

Although “breast stroke” or “rowing” is a frequently reported locomotion mode in five-armed brittle stars, some studies have also described patterns in which there is no leading arm. One of these patterns is “paddling” or “reverse rowing”, and it occurs when a backmost arm is dragged while the other four actively row (Preyer, 1887; Uexküll, 1905; Glaser, 1907; Arshavskii et al., 1976a; Astley, 2012). Such patterns without leading arms have been observed during free movement without experimental

stimuli (Arshavskii et al., 1976a; Astley, 2012) as well as during escape behaviour for a short time (Yee et al., 1987). In our study using *O. brachyaspis*, each trial seldom showed such a non-leading pattern (Figs S1–S4). Assuming that this species uses different locomotion modes, non-leading patterns might be employed only for several seconds after stimuli. In this case, we may have overlooked or underestimated this phase in the present study since we uniformly analysed one-minute duration after the beginning of the disk's movement. Still, considering the fixed period for which post-stimulus locomotion was herein quantified, it seems that locomotion using a leading arm is more common mode in the intact individuals of *Ophiactis* species regardless of their number of arms.

Deciding moving direction

Since brittle stars show no consistent front in behavioural terms, as most echinoderms, every arm can be a leading arm. Astley (2012) described their turning behaviour in a short-term series, which was performed by changing the roles of arms rather than by rotating their body axis. Regarding escape situations, studies have reported that brittle stars avoid open or bright spaces (Cowles, 1910; Matsuzaka et al., 2017), predator extracts (Yee et al., 1987), and KCl solution (Clark et al., 2019; Kano et al., 2019). However, few studies have focused on how each arm reacts to such repellents and defines the direction of the movement of an individual. Since light and liquid diffuse in water, it is difficult to stimulate only a single target arm. Especially for small brittle stars such as *Ophiactis* species, tactile stimulation would perform effectively for the aim to understand how signals from a stimulated arm affect the movements of the other arms.

In our study, two quantitative indices calculated from the filtered angular velocity of arms—B_α and $E_{\alpha\beta}$—and one obtained from the original coordinate data—Θ—allowed us to visualize ophiuroid locomotion without contradiction (Figs 5–8). By postulating each average of the two Θ_{sign}-based patterns as a representative, our numerical results indicated that the most frequent locomotion pattern after aversive tactile stimulation is the following: a leading arm emerges at the *second* neighbour of a stimulated arm, while side arms adjacent to the leader synchronously push backward, no matter how many arms a brittle star has. To perform this bilateral distribution with a

high probability, it can be assumed that an afferent signal from an arm induces one of the *first* neighbouring arms to be an active rower that pushes in the direction of the signalling arm, while the *second* neighbouring arm is an inactive one and has a less important directional preference, and the *third* neighbouring arm is active and pushes synchronously but oppositely to the *first*'s pushing (Fig. 9). Accordingly, the *second* arm faces forward while the *first*, *third*, and some rear arms work on the individuals both sides.

Kano et al. (2019) proposed a model in which arm movements become potentially symmetrical to aversive stimulation. We initially expected such a symmetrical scheme to allow the animal to escape opposite to the stimulus. However, our study demonstrates that the aversive signal makes an asymmetrical effect on either direction. In our model, whether the clockwise or anticlockwise *second* arm becomes a leading arm depends on which direction the signal from the stimulated arm dominantly transfers. This either-or choice would be caused by asymmetry in a body posture or outer environment at the moment of stimulation. In particular, the bimodality in the seven-armed individual (Fig. 4D) could be an evidence that one individual determines either trial-by-trial. This mechanism of decision making should be further investigated. The apparent randomness might be beneficial in the escape behaviour because it would be difficult for a predator to predict in which direction a brittle star will move.

Under our model shown in Fig. 9, brittle stars with more arms have a higher risk of approaching a threat such as a predator. If the front is placed ideally around the *second* neighbouring arm from the stimulus, four-, five-, six-, and seven-armed animals will respectively show 0, 36, 60, and 77 deg in average $|\Theta|$. In fact, the estimation from the measured data was similar—17, 29, 46, and 70 deg, respectively—, and trials in which moving direction inclined toward the stimulated arm ($90 < |\Theta| \leq 180$) were more frequent as the tested body had more arms: 0/15, 1/30, 3/30, and 5/15, respectively (Fig. 4). Although this behaviour as a response to a threat is considered less adaptive, an evolutionary background would explain it. It has been proposed that primitive ophiuroids showed pentaradial symmetry (Paul and Smith, 1984; Sumrall and Wray, 2007), implying that brittle stars had developed a locomotion mechanism which worked optimally for the five-armed body. Some exceptional individuals in arm number, at least the four-, six-, and seven-armed bodies, probably have kept following this initial plan

without vital issues. Meanwhile, escape direction may be more or less inclined as a side effect, and the minority of four- and seven-armed ones might be a reflection of some inconvenience in control mechanism or its resultant behaviour.

Our study provides important information on how behavioural direction is expressed in a body without antero-posterior and left-right axes. Even when the individual's body is round, some direction-making signal could transfer linearly in one direction at a local view on the circumference (Fig. 9), just like a wave on a string or neural transmission in the spinal cord. If brittle stars indeed use this strategy, the number of segments with identical function in the pathway is not important.

Inter-arm interaction

The inter-arm connection depicted in Fig. 9 is recognizable as the circumoral nerve ring, i.e., the main portion of the nervous system that runs in the disk. This correspondence is indicated by its orbital morphology as well as previous studies that support the importance of the nerve ring in locomotion (Mangold, 1909; Diebschlag, 1938; Arshavskii et al., 1976a,b; Matsuzaka et al., 2017; Clark et al., 2019; Kano et al., 2019). Although it is difficult to measure neural activity in the small body of *Ophiactis* species, such an internal neural network can be suggested from behavioural modelling based on external observation. Given the simplicity of the ophiuroid nervous system, we can assume that the movement of each arm directly reflects neural activity in each unit, which could also be explained by a couple of neurons. For instance, the observed locomotion can be used for testing "neuron ring" models (Suzuki et al., 1971; Matsuoka, 1985) and the functioning of circularly arranged neurons. The unique variability of fissiparous brittle stars allows us to test the function of different numbers of neurons, connecting theoretical biology and experimental biology.

Besides the crucial role of neural interactions, Kano et al. (2017) identified the ophiuroids' ability to immediately change their locomotion patterns after losing some arms and built an ophiuroid-like robot that imitated the animal's adaptive locomotion via a local feedback without pre-programmed control. Other robotics studies have also suggested the importance of 'physical' interactions in movement coordination which is independent of electrical circuits (Owaki et al., 2013; Owaki and Ishiguro, 2017). The results of these studies indicate that four- to seven-armed individuals are not likely to

553 employ different central control systems while counting the total number of arms. Each
554 functional unit—e.g., each arm and each branch of the nerve ring—would refer to the
555 states of its nearest-neighbour units while ignoring distant ones; nevertheless, a
556 coordinated pattern casually arises at a level of individual, no matter how many units
557 they own. In this perspective, the worse performance of the individuality-assuming
558 model (Table 1) implies that an important structural hierarchy for a brittle star might be
559 each unit rather than an individual body. A trial-by-trial variability in moving direction
560 and other indices (Figs S1–S4) might reflect the influence of physical properties such as
561 arms' posture at each moment, although a circular neural network would chiefly design
562 the average orientation, in which the stimulated arm's *second* neighbour faces forward
563 (Fig. 9).
564 Except for the unexpected escape direction in the more-armed cases, the
565 resultant concept fits our initial hypothesis in terms of a decentralized design. The high
566 independence among body sectors may have contributed to ophiuroid evolution and
567 allowed variability in appendage number. This may be a reason why some species such
568 as *Ophiactis brachyaspis* have acquired fissiparity, being capable of drastic
569 morphological changes in a life cycle while retaining its locomotive ability. The unique
570 'non-brained' strategy of fissiparous brittle stars may serve as a base for a highly
571 flexible design in robotics. More specifically, multi-directional robots may imitate the
572 ophiuroid model's high mobility in every horizontal direction while promptly reacting
573 to external stimuli.
574
575 **Limitations**
576 Although we conducted behavioural experiments on a flat acrylic surface, *Ophiactis*
577 brittle stars typically inhabit rough rocky surfaces. They lay some arms in interstices
578 while raising some arms from the substrate (personal observation); suspension-feeding
579 ophiuroids commonly show this posture (Warner, 1971). In their habitats, ophiuroids'
580 arms may not be chiefly used for locomotion, and escaping direction may depend on
581 their posture at each moment. Thus, our model should be further tested using ophiuroid
582 species that live on bottom surfaces and have active locomotion, such as *Ophiura* and
583 *Ophiarachna*. However, these non-fissiparous brittle stars have low variability in
584 number of arms, and thus we should investigate a large number of five-armed

specimens to analyse their potential bimodality in locomotion.

Intact individuals with other than five or six arms are rare even among fissiparous brittle stars. Although we observed only one specimen with four arms and one with seven arms, we believe that the bias caused by individual selection was not large given the good performance of the non-individuality model in five- and six-armed individuals' movements. Still, ideally, rare cases should also be further investigated using large sample sizes to consolidate our model.

Finally, the fissiparous brittle stars collected in the same aquarium might be clones resulting from the asexual reproduction of a single individual. It is possible that locomotion is affected by genotype, and this may reflect the high support of the non-individuality model. Further studies sampling individuals from different localities would solve this issue.

Acknowledgments

Our deepest appreciation goes to Mr. Keita Harada in Shirahama Aquarium, Kyoto University, for sending us the fresh individuals of brittle stars from the aquarium. We are grateful to the member of Stan Community (https://mc-stan.org/community/) for suggesting improved methods of statistical modelling. We would like to thank Editage (www.editage.com) for English language editing.

Funding

This work was partly supported by JSPS KAKENHI (grant number 16KT0099) and by JST CREST (grant number JPMJCR14D5), Japan.

Ethics

This article does not present research with ethical considerations.

Data, code and materials

The preprint of this article is available in BioRxiv (Wakita et al., 2019a). The datasets generated and/or analysed during the current study are available in the Figshare repository (Wakita et al., 2019b).

Competing interests

The authors declare that they have no competing interests.

Authors' contributions

DW and HA designed the study and conducted behavioural experiments and measurements. DW and KK performed statistical modelling. All authors wrote the manuscript and approved the final manuscript.

References

Arshavskii, Yu. I., Kashin, S. M., Litvinova, N. M., Orlovskii, G. N. and Fel'dman, A. G. (1976a). Types of locomotion in ophiurans. *Neurophysiology* **8**, 398−404.

Arshavskii, Yu. I., Kashin, S. M., Litvinova, N. M., Orlovskii, G. N. and Fel'dman, A. G. (1976b). Coordination of arm movement during locomotion in ophiurans. *Neurophysiology* **8**, 404−410.

Astley, H. C. (2012). Getting around when you're round: quantitative analysis of the locomotion of the blunt-spined brittle star, *Ophiocoma echinata*. *J. Exp. Biol.* **215**, 1923–1929.

Boffi, E. (1972). Ecological aspects of ophiuroids from the phytal of SW Atlantic Ocean warm waters. *Mar. Biol.* **15**, 316–328.

Bremaeker, N. D., Deheyn, D., Thorndyke, M. C., Baguet, F. and Mallefet, J. (1997). Localization of S1- and S2-like immunoreactivity in the nervous system of the brittle star *Amphipholis squamata* (Delle Chiaje 1828). *Proc. Royal Soc. B* **264**, 667–674.

Clark, E. G., Kanauchi, D., Kano, T., Aonuma, H., Briggs, D. E. and Ishiguro, A. (2019). The function of the ophiuroid nerve ring: how a decentralized nervous system controls coordinated locomotion. *J. Exp. Biol.* **222**, jeb192104.

Cobb, J. L. and Stubbs, T. R. (1981). The giant neurone system in ophiuroids I: the general morphology of the radial nerve cords and circumoral nerve ring. *Cell Tissue Res.* **219**, 197–207.

Cobb, J. L. and Stubbs, T. R. (1982). The giant neurone system in ophiuroids III: the

649 detailed connections of the circumoral nerve ring. *Cell Tissue Res.* **226**, 675–687.
650 Cowles, R. P. (1910). Stimuli produced by light and by contact with solid walls as
651 factors in the behavior of ophiuroids. *J. Exp. Zool.* **9**, 387–416.
652 Diebschlag, E. (1938). Ganzheitliches verhalten und lernen bei echinodermen. *Z. Vergl.*
653 *Physiol.* **25**, 612–654.
654 Gelman, A., Stern, H. S., Carlin, J. B., Dunson, D. B., Vehtari, A. and Rubin, D. B.
655 (2013). *Bayesian Data Analysis*. 3rd edition. Florida, USA: CRC Press.
656 Ghyoot, M., Cobb, J. L. S. and Thorndyke, M. C. (1994). Localization of neuropeptides
657 in the nervous system of the brittle star *Ophiura ophiura*. *Philos. Trans. Royal Soc.*
658 *B* **346**, 433–444.
659 Glaser, O. C. (1907). Movement and problem solving in *Ophiura brevispina*. *J. Exp.*
660 *Zool.* **4**, 203–220.
661 Hoffman, M. D. and Gelman, A. (2014). The No-U-Turn sampler: adaptively setting
662 path lengths in Hamiltonian Monte Carlo. *J. Mach. Learn. Res.* **15**, 1593–1623.
663 Kano, T., Sato, E., Ono, T., Aonuma, H., Matsuzaka, Y. and Ishiguro, A. (2017). A
664 brittle star-like robot capable of immediately adapting to unexpected physical
665 damage. *Royal Soc. Open Sci.* **4**, 171200.
666 Kano, T., Kanauchi, D., Aonuma, H., Clark, E. G., and Ishiguro, A. (2019).
667 Decentralized control mechanism for determination of moving direction in brittle
668 stars with penta-radially symmetric body. *Front. Neurorobot.* **13**, 66.
669 Mangold, E. (1909). Studien zur physiologie des nervensystems der echinodermen.
670 *Pflug. Arch. Eur. J. Phy.* **126**, 371–406.
671 Matsuoka, K. (1985). Sustained oscillations generated by mutually inhibiting neurons
672 with adaptation. *Biol. Cybern.* **52**, 367–376.
673 Matsuzaka, Y., Sato, E., Kano, T., Aonuma, H. and Ishiguro, A. (2017). Non-
674 centralized and functionally localized nervous system of ophiuroids: evidence from
675 topical anesthetic experiments. *Biol. Open* **6**, 425–438.
676 Mladenov, P. V. and Emson, R. H. (1984). Divide and broadcast: sexual reproduction in
677 the West Indian brittle star *Ophiocomella ophiactoides* and its relationship to
678 fissiparity. *Mar. Biol.* **81**, 273–282.
679 Mladenov, P. V., Emson, R. H., Colpit, L. V. and Wilkie, I. C. (1983). Asexual
680 reproduction in the West Indian brittle star *Ophiocomella ophiactoides* (H.L. Clark)

(Echinodermata: Ophiuroidea). *J. Exp. Mar. Biol. Ecol.* **72**, 1–23.

Owaki, D. and Ishiguro, A. (2017). A quadruped robot exhibiting spontaneous gait transitions from walking to trotting to galloping. *Sci. Rep.* **7**, 277.

Owaki, D., Kano, T., Nagasawa, K., Tero, A. and Ishiguro, A. (2013). Simple robot suggests physical interlimb communication is essential for quadruped walking. *J. Royal Soc. Interface* **10**, 20120669.

Paul, C. R. C. and Smith, A. B. (1984). The early radiation and phylogeny of echinoderms. *Biol. Rev.* **59**, 443–481.

Preyer, W. T. (1887). *Die Bewegungen der Seesterne*. Berlin, Germany: Friedländer.

R Core Team (2018). R: a language and environment for statistical computing. https://www.R-project.org. Accessed 15 November 2018.

Romanes, G. J. and Ewart, J. C. (1881). Observations on the locomotor system of Echinodermata. *Philos. Trans. Royal Soc.* **172**, 829–885.

Stan Development Team (2018). Stan modeling language users guide and reference manual, version 2.18.0. http://mc-stan.org. Accessed 15 November 2018.

Sumrall, C. D. and Wray, G. A. (2007). Ontogeny in the fossil record: diversification of body plans and the evolution of “aberrant” symmetry in Paleozoic echinoderms. *Paleobiology* **33**, 149–163.

Suzuki, R., Katsuno, I. and Matano, K. (1971). Dynamics of “neuron ring”. *Kybernetik* **8**, 39–45.

Uexküll, J. V. (1905). Studien über den tonus II: die bewegungen der schlangensterne. *Z. Biol.* **46**, 1–37.

Wakita, D., Kagaya, K. and Aonuma, H. (2019a). Generalized locomotion of brittle stars with a flexible number of arms. *bioRxiv*. https://doi.org/10.1101/616383.

Wakita, D., Kagaya, K. and Aonuma, H. (2019b). Data from: Data and codes of “A general model of locomotion of brittle stars with a variable number of arms”. *Figshare*. https://doi.org/10.6084/m9.figshare.8019827.v4.

Warner, G. F. (1971). On the ecology of a dense bed of the brittle-star *Ophiothrix fragilis*. *J. Mar. Biol. Assoc. U.K.* **51**, 267–282.

Watanabe, S. (2009). *Algebraic Geometry and Statistical Learning Theory*. Cambridge, UK: Cambridge University Press.

Watanabe, S. (2010). Asymptotic equivalence of Bayes cross validation and widely

applicable information criterion in singular learning theory. *J. Mach. Learn. Res.* **11**, 3571–3594.

Watanabe, S. (2018). *Mathematical Theory of Bayesian Statistics*. Florida, USA: CRC Press.

Watanabe, W., Kano, T., Suzuki, S. and Ishiguro, A. (2011). A decentralized control scheme for orchestrating versatile arm movements in ophiuroid omnidirectional locomotion. *J. Royal Soc. Interface* **9**, 102–109.

Yee, A., Burkhardt, J. and Gilly, W. F. (1987). Mobilization of a coordinated escape response by giant axons in the ophiuroid, *Ophiopteris papillosa*. *J. Exp. Biol.* **128**, 287–305.

Zueva, O., Khoury, M., Heinzeller, T., Mashanova, D. and Mashanov, V. (2018). The complex simplicity of the brittle star nervous system. *Front. Zool.* **15**, 1.

Figure captions

Fig. 1. The fissiparous brittle star *Ophiactis brachyaspis*. A: a five-armed individual. B: a six-armed individual. The scale bar represents 2 mm.

Fig. 2. Measurements of the locomotion of a brittle star (*Ophiactis brachyaspis*). Schematic five-armed brittle stars are shown at the first (t = 1), t-th, and last (t = 600) frames as an example. Not all arms are shown except for the first frame. The arm index, α, takes the values of 1 to 5, in which the stimulated arm is numbered 1. Blue-filled circles indicate the coordinate points of $P'_\alpha(t)$, while open circles show those of $P_\alpha(t)$. $P_1(t)$ is indicated by red-lined open circles. The centre of gravity of $P_\alpha(t)$, namely $P_{\mathrm{cent}}(t)$, is represented by red-lined filled circles. $\varphi_\alpha(t)$ is the arm angle formed by $P_\alpha(t)$, $P_{\mathrm{cent}}(t)$, and $P'_\alpha(t)$. $\theta(t)$ is the angle formed by the segment $P_{\mathrm{cent}}(1)P_{\mathrm{cent}}(600)$ and $P_1(t)P_{\mathrm{cent}}(t)$, representing the direction of the stimulated arm compared to the moving direction. The moving distance S corresponds to the length of the segment $P_{\mathrm{cent}}(1)P_{\mathrm{cent}}(600)$.

Fig. 3. Calculation and visualization of the locomotion of a five-armed brittle star (*Ophiactis brachyaspis*). A: temporal change of $\varphi_\alpha(t)$ (deg) (c.f. Fig. 2). B: temporal change of $\omega_\alpha(t)$ (deg/s)—angular velocity of $\varphi_\alpha(t)$. Background grey plots represent the original data, while thicker blue plots show low-pass filtered data. Each plot's "mean" indicates the mean value of the filtered $\omega_\alpha(t)$ for t = 1, 2, ..., 600. C: temporal change of signed $\omega_\alpha(t)^2$. Each plots' "mean" indicates its mean value for t = 1, 2, ..., 600, corresponding to B_α—the tendency of being a left or right rower in the α-th arm (Equation 3). D: temporal change of $\theta(t)$ (deg) (c.f. Fig. 2). "Mean" indicates its mean value for t = 1, 2, ..., 600, corresponding to Θ (deg)—moving direction (Equation 1). E: schematized brittle star reflecting the mean $\omega_\alpha(t)$ calculated in B and Θ in D. F: schematized brittle star reflecting B_α in C and Θ in D. In E and F, each grey arrowhead indicates the stimulated arm numbered 1, with the numbers following in order anticlockwise. The angles of black arrows at the disks represent Θ. Arms with negative/positive mean values extend blue-leftward/red-rightward arrows, respectively, with the arrows' length corresponding to the absolute value of its mean. Compared to

the mean values of the original $\omega_\alpha(t)$ in E, B_α in F well explains actual locomotion (c.f. Video S1). Note that B_α originally reflects a returning direction based on its sign (positive B_α denotes anticlockwise returning), but its schematized arrow indicates a 'pushing direction' for simply imagining force to the ground (positive B_α denotes clockwise pushing, thus apparently opposing the sign in Fig. 2). Scale bars represent 1.0 for the mean $\omega_\alpha(t)$ in E and 20 for B_α in F.

Fig. 4. Circular plots of moving direction after aversive tactile stimulation in brittle stars (*Ophiactis brachyaspis*). A: five-armed case (10 individuals, 30 trials). B: six-armed case (10 individuals, 30 trials). C: four-armed case (one individual, 15 trials). D: seven-armed case (one individual, 15 trials). The moving direction Θ is the measured angle based on the position of a mechanically stimulated arm (c.f. Figs 2, 3, Equation 1). Θ is 0 deg when the disk moves in the opposite direction to the stimulated arm, and is negative/positive when the disk movement is angled clockwise/anticlockwise, respectively, from the 0 deg. Each point represents Θ in each trial, which is grouped in a bin divided per 22.5 deg. Density plots on the background represent predictive distributions on the assumption of two symmetrical von Mises distributions.

Fig. 5. Locomotion of five-armed brittle stars (*Ophiactis brachyaspis*) grouped by moving direction. A, B: case in which moving direction (Θ; c.f. Figs 2, 3, Equation 1) is angled clockwise from the opposite direction to the stimulated arm, i.e., Θ is negative and $\Theta_{\mathrm{sign}} = 0$ (eight individuals, 11 trials). C, D: case in which Θ is positive (angled clockwise), i.e., $\Theta_{\mathrm{sign}} = 1$ (10 individuals, 19 trials); an example is shown in Video S1. A, C: schematized brittle stars reflecting the resultant quantitative values. Black arrows at the disks represent the measured means of moving distance (S; c.f. Fig. 2) by length and the measured means of Θ by angle. Error bars parallel to the disks' arrows show S's standard deviation (s.d.), and arc-shaped error bars represent Θ's s.d. in data. The blue or red arrow at each arm represents the tendency of being a left or right rower (B_α; c.f. Figs 2, 3, Equation 3), reflecting the absolute median of each posterior mean by arrow length and the median of each posterior s.d. by error bars. When a posterior mean was negative/positive, its blue-leftward/red-rightward arrow extends from its arm, indicating that the arm pushed leftward/rightward (anticlockwise/clockwise), respectively. In each

panel, the arm with the maximum absolute value in posterior mean is coloured with the darkest blue/red, while the other arms show lighter blue/red corresponding to the relative values to the maximum. Scale bars represent 40 mm for S and 50 for B_α. Trial-by-trial diagrams are shown in Fig. S1. B, D: degree of synchronization between two arms ($E_{\alpha\beta}$ for the α- and β-th arms; Equation 4). Small circles represent measured data. Pair-by-pair red pluses indicate the medians of posterior means, while error bars show the medians of posterior s.d. parameters. Negative/positive values represent that the paired movement of the α- and β-th arms synchronized in the opposite/same direction, respectively. Each asterisk indicates the pair with the largest negative estimated mean, showing remarkable antiphase synchronization. These pairs correspond to those with strong average leftward/rightward biases in A and C. All posterior distributions for both B_α and $E_{\alpha\beta}$ were estimated under a best performed model in terms of WAIC, in which Θ_{sign} is an explanatory variable for the mean and s.d.

Fig. 6. Locomotion of six-armed brittle stars (*Ophiactis brachyaspis*) grouped by moving direction. A, B: case in which $\Theta_{\mathrm{sign}} = 0$ (eight individuals, 16 trials). C, D: case in which $\Theta_{\mathrm{sign}} = 1$ (eight individuals, 14 trials); an example is shown in Video S2. A, C: schematized brittle stars reflecting the resultant quantitative values, as explained in Fig. 5. Trial-by-trial diagrams are shown in Fig. S2. B,D: degree of synchronization between two arms ($E_{\alpha\beta}$ for the α- and β-th arms; Equation 4), as explained in Fig. 5.

Fig. 7. Locomotion of four-armed brittle star (*Ophiactis brachyaspis*) grouped by moving direction. A, B: case in which $\Theta_{\mathrm{sign}} = 0$ (one individuals, eight trials). C, D: case in which $\Theta_{\mathrm{sign}} = 1$ (one individuals, seven trials). A, C: schematized brittle stars reflecting the resultant quantitative values, as explained in Fig. 5. Trial-by-trial diagrams are shown in Fig. S3. B, D: degree of synchronization between two arms ($E_{\alpha\beta}$ for the α- and β-th arms; Equation 4), as explained in Fig. 5.

Fig. 8. Locomotion of seven-armed brittle star (*Ophiactis brachyaspis*) grouped by moving direction. A, B: case in which $\Theta_{\mathrm{sign}} = 0$ (one individuals, eight trials). C, D: case in which $\Theta_{\mathrm{sign}} = 1$ (one individuals, seven trials). A, C: schematized brittle stars reflecting the resultant quantitative values, as explained in Fig. 5. Trial-by-trial

822 diagrams are shown in Fig. S4. B, D: degree of synchronization between two arms ($E_{\alpha\beta}$
823 for the α- and β-th arms; Equation 4), as explained in Fig. 5.
824
825 **Fig. 9. Model of arm-by-arm locomotive movements in brittle stars with a variable**
826 **number of arms after aversive tactile stimulation.** The stimulated arm makes an
827 afferent signal—(A)—which chiefly transfers through inter-arm connections (clockwise
828 or anticlockwise), represented by the circumoral nerve ring. The direction in which the
829 signal dominates is determined by some perturbation—(B). Subsequently, one of the
830 *first* neighbouring arms to the stimulated arm actively pushes the ground in the stimulus
831 direction, while the *third* neighbour (in the same direction) synchronously pushes in the
832 opposite direction to the *first*. As a result, the *second* arm between the *first* and *third*
833 faces forward in behavioural terms—(C) or (C′).
834

Tables

Table 1. WAICs of statistical models for Θ, B_α, and $E_{\alpha\beta}$.

Model	Specification		Four-armed			Five-armed			Six-armed			Seven-armed		
			Rank	WAIC	Δ	Rank	WAIC	Δ	Rank	WAIC	Δ	Rank	WAIC	Δ
Θ	Distribution number													
1	one		2	0.876	0.917	2	1.192	0.764	2	1.518	5.55	2	1.860	10.7
2	two		1	0.845	**0***	1	1.179	**0***	1	1.425	**0***	1	1.502	**0***
B_α	Explanatory variable†	Individuality†												
1	no	no	3	4.217	4.94	8	4.671	60.4	5	5.338	58.9	4	4.940	25.7
2	no	yes	—	—	—	9	4.676	61.9	10	5.352	64.0	—	—	—
3	L_α	no	1	4.176	**0***	10	4.679	62.9	9	5.350	63.2	5	4.956	29.0
4	L_α	yes	—	—	—	12	4.688	65.4	12	5.382	74.9	—	—	—
5	S	no	5	4.267	10.9	7	4.670	60.3	7	5.338	59.2	3	4.879	12.8
6	S	yes	—	—	—	11	4.680	63.1	11	5.360	67.0	—	—	—
7	Θ	no	2	4.187	1.29	1	4.469	**0***	2	5.191	6.25	2	4.827	2.03
8	Θ	yes	—	—	—	2	4.477	2.16	4	5.208	12.2	—	—	—
9	Θ_{sign}	no	4	4.230	6.41	3	4.501	9.43	1	5.174	**0***	1	4.818	**0***
10	Θ_{sign}	yes	—	—	—	4	4.505	10.8	3	5.193	6.89	—	—	—
11	F_α	no	6	4.271	11.3	5	4.640	51.0	6	5.338	59.1	6	4.955	28.8
12	F_α	yes	—	—	—	6	4.644	52.3	8	5.347	62.4	—	—	—
$E_{\alpha\beta}$	Explanatory variable†													
1	no		1	3.951	**0***	4	4.327	25.6	4	4.440	42.0	3	4.294	9.30
2	S		4	3.974	4.14	3	4.321	22.0	2	4.413	17.5	4	4.308	18.0
3	Θ		2	3.953	0.365	2	4.292	4.90	3	4.416	20.0	2	4.282	1.58
4	Θ_{sign}		3	3.959	1.45	1	4.284	**0***	1	4.394	**0***	1	4.279	**0***

*Δ = 0 (bolded) indicates a best supportive model. †"No" indicates individuality was not considered; otherwise, it was considered in the mean of normal distribution.

Fig. 1

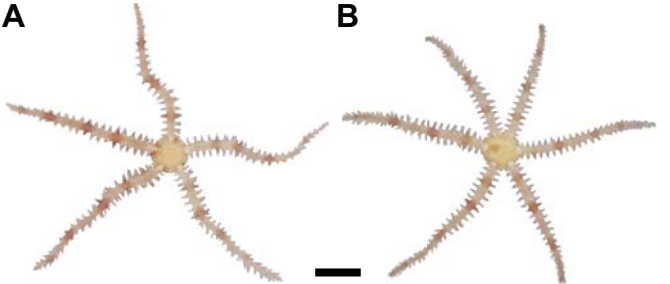

Fig. 2

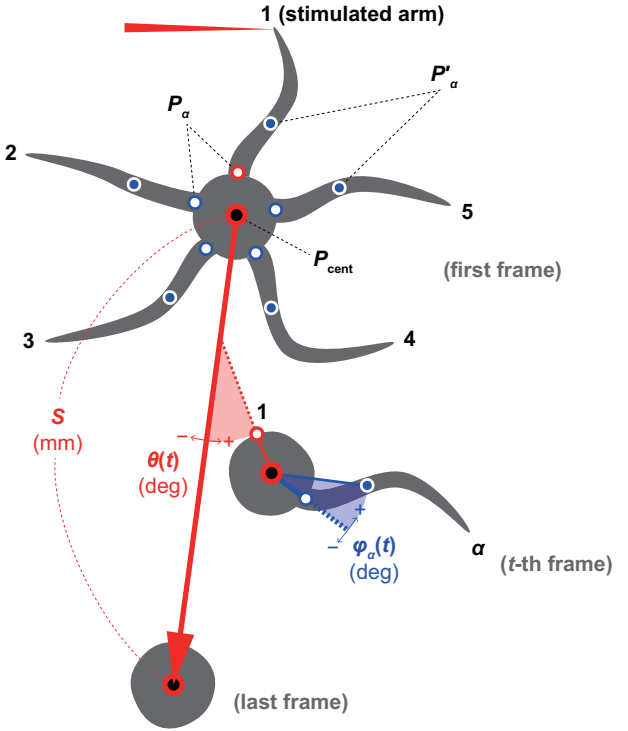
1 (stimulated arm)
P'α
Pα
2
5
Pcent
(first frame)
3
4
S
(mm)
1
θ(t)
(deg)
φα(t)
(deg)
α
(t-th frame)
(last frame)

Fig. 3

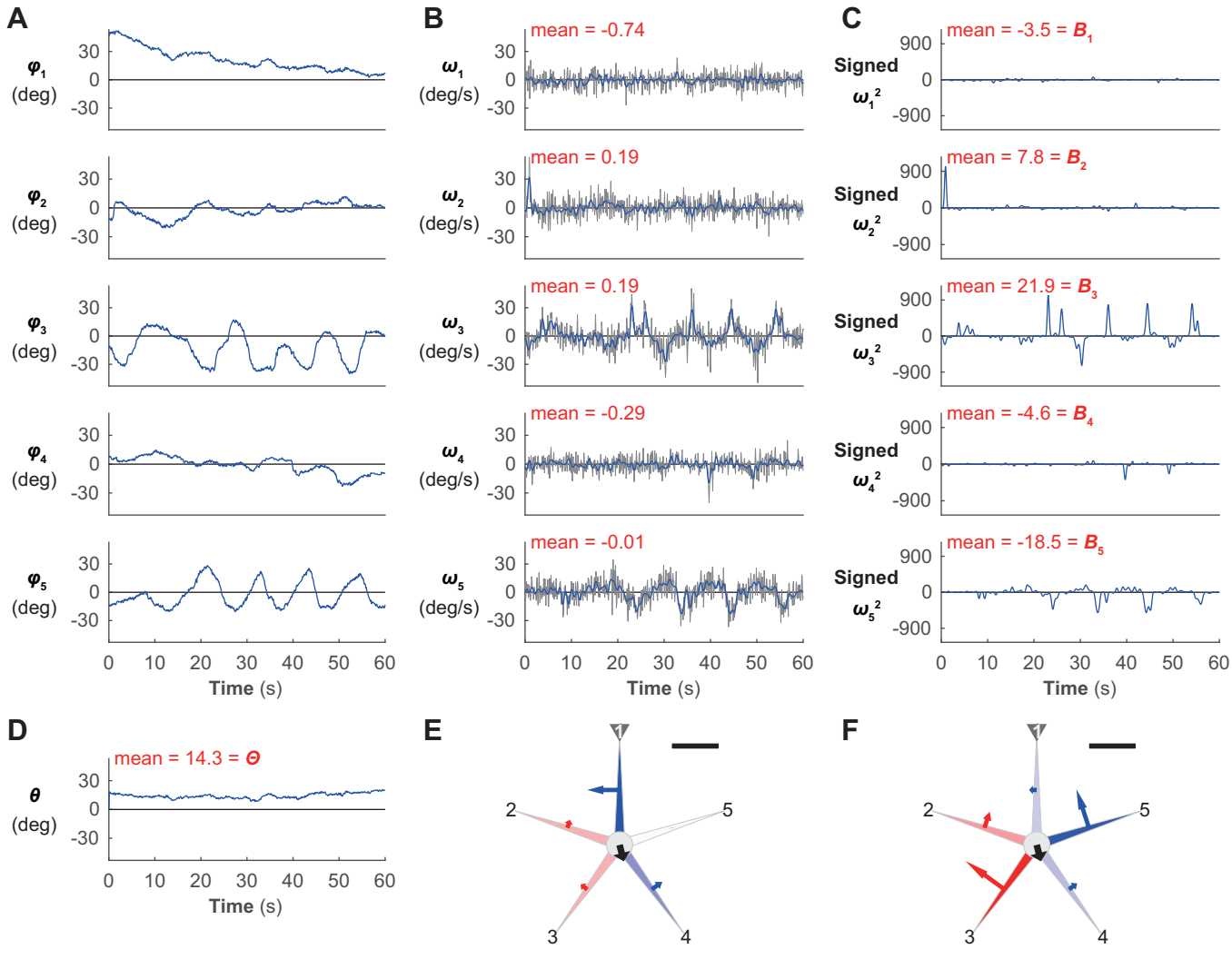
A
B
C
D
E
F
φ_1 (deg)
φ_2 (deg)
φ_3 (deg)
φ_4 (deg)
φ_5 (deg)
ω_1 (deg/s)
ω_2 (deg/s)
ω_3 (deg/s)
ω_4 (deg/s)
ω_5 (deg/s)
mean = -0.74
mean = 0.19
mean = 0.19
mean = -0.29
mean = -0.01
Signed ω_1^2
Signed ω_2^2
Signed ω_3^2
Signed ω_4^2
Signed ω_5^2
mean = -3.5 = B_1
mean = 7.8 = B_2
mean = 21.9 = B_3
mean = -4.6 = B_4
mean = -18.5 = B_5
θ (deg)
mean = 14.3 = Θ
Time (s)
2
3
4
5

Fig. 4

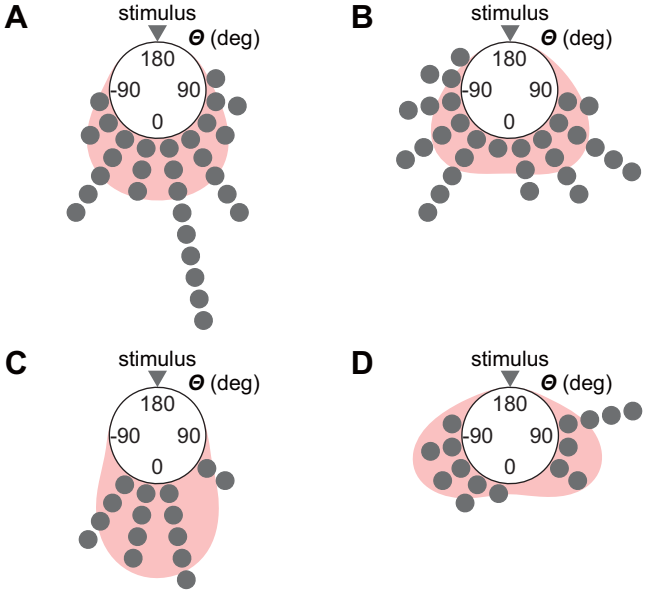
A
stimulus
Θ (deg)
180
-90
90
0
B
stimulus
Θ (deg)
180
-90
90
0
C
stimulus
Θ (deg)
180
-90
90
0
D
stimulus
Θ (deg)
180
-90
90
0

Fig. 5

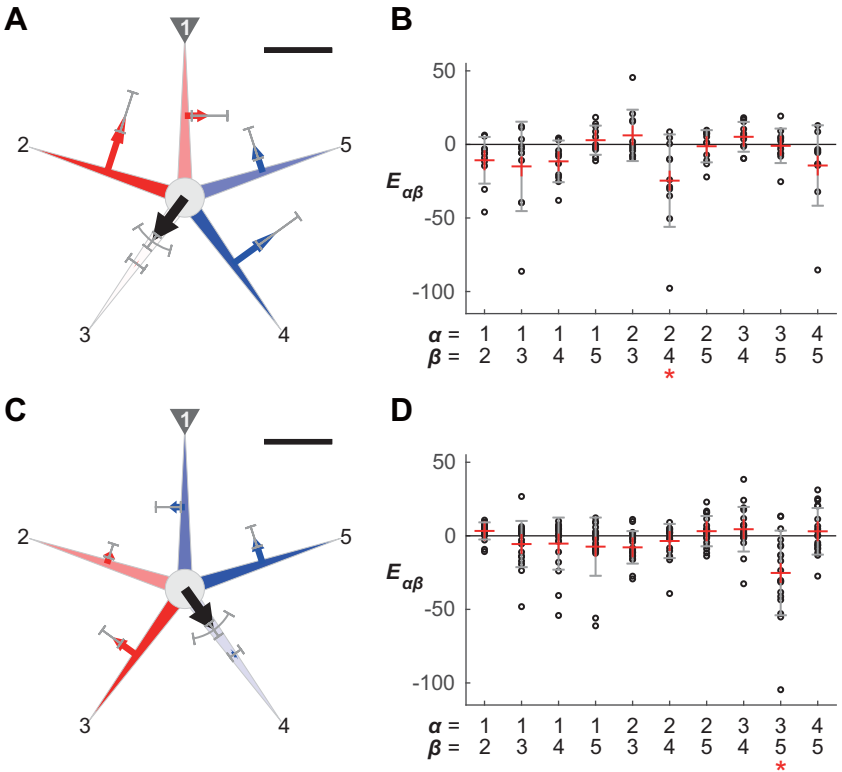
A
1
2
5
3
4
B
50
0
-50
-100
$E_{\alpha\beta}$
α = 1 1 1 1 2 2 2 3 3 4
β = 2 3 4 5 3 4 5 4 5 5
*
C
1
2
5
3
4
D
50
0
-50
-100
$E_{\alpha\beta}$
α = 1 1 1 1 2 2 2 3 3 4
β = 2 3 4 5 3 4 5 4 5 5
*

Fig. 6

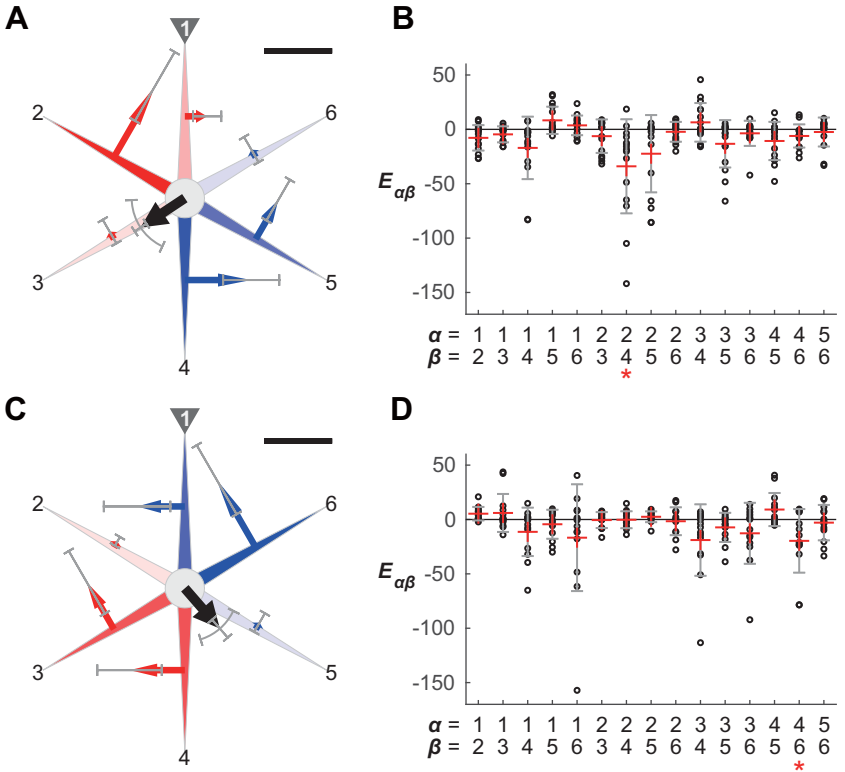
A
1
2
3
4
5
6
B
50
0
-50
-100
-150
$E_{\alpha\beta}$
α = 1 1 1 1 1 2 2 2 2 3 3 3 4 5 5
β = 2 3 4 5 6 3 4 5 6 4 5 6 6 6 6
*
C
1
2
3
4
5
6
D
50
0
-50
-100
-150
$E_{\alpha\beta}$
α = 1 1 1 1 1 2 2 2 2 3 3 3 4 5 5
β = 2 3 4 5 6 3 4 5 6 4 5 6 6 6 6
*

Fig. 7

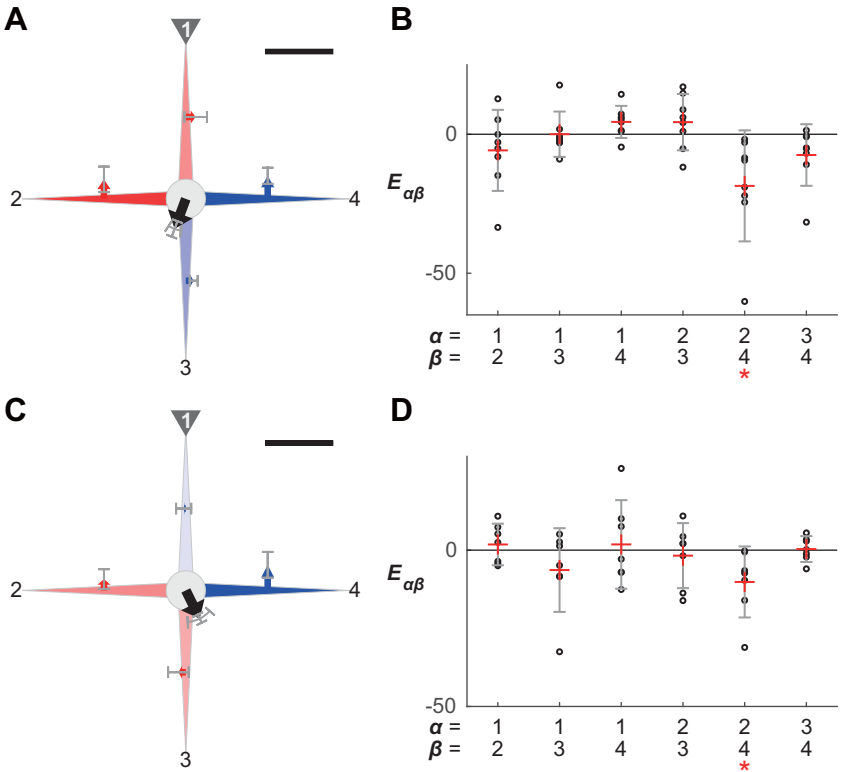
A
1
2
3
4
B
0
-50
$E_{\alpha\beta}$
α = 1 1 1 2 2 3
β = 2 3 4 3 4 4
*
C
1
2
3
4
D
0
-50
$E_{\alpha\beta}$
α = 1 1 1 2 2 3
β = 2 3 4 3 4 4
*

Fig. 8

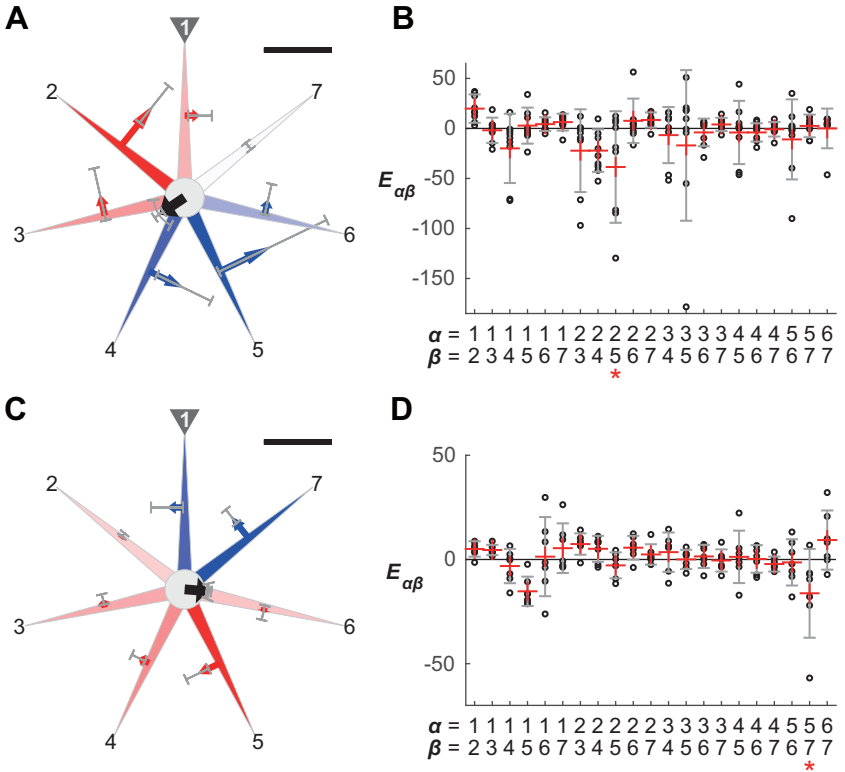
A
1
2
7
3
6
4
5
B
50
0
-50
-100
-150
$E_{\alpha\beta}$
α = 1 1 1 1 1 1 2 2 2 2 2 3 3 3 4 4 4 5 5 6
β = 2 3 4 5 6 7 3 4 5 6 7 4 5 6 5 6 7 6 7 7
*
C
1
2
7
3
6
4
5
D
50
0
-50
$E_{\alpha\beta}$
α = 1 1 1 1 1 1 2 2 2 2 2 3 3 3 4 4 4 5 5 6
β = 2 3 4 5 6 7 3 4 5 6 7 4 5 6 5 6 7 6 7 7
*